Nanotechnology

DOI: 10.1002/anie.201004220

Tunable Nanosynthesis of Composite Materials by Electron-Impact Reaction**

*Laurent Bernau, Mihai Gabureac, Rolf Erni, and Ivo Utke**

Nanoscale electron-induced reactions being triggered by a finely focused electron beam in modern scanning electron microscopes are commonly used to pattern surfaces of thin films of irradiation sensitive material. Classical polymer and inorganic resist films allow precise masks to be defined for further deposition or etching process steps in the semiconductor industry.[1] A new, promising approach employs new film materials, among which are self-assembled monolayers of biphenyl, passivated gold nanoclusters, Langmuir–Blodgett films, or liquid precursors. The exposure of these films to electrons directly results in membranes, electrical wires, plasmonic structures, or conducting dots with nanoscale dimensions.[2]

A very promising approach to electron-impact nanosynthesis is to replace the solid or liquid film and use a physisorbed monolayer that is continuously refreshed by injected volatile molecules.[3] The process can be compared to local chemical vapor deposition; however, the decomposition is due to electron-impact dissociation rather than thermal dissociation, thus keeping the reaction confined to the size of the electron beam and the active electron interaction volume. It has been proven to be a very innovative concept for direct, local, three-dimensional, and minimally invasive nanosynthesis of future photonic,[4] electronic,[5] and mechanical[6] nanodevice materials as well as for site-specific patterning of catalyst for individual carbon nanotube growth[7] and atomic layer deposition.[8] For nanoscale deposition, a focused electron beam is usually scanned over surface-adsorbed metal containing compounds that are volatile at room temperature. Electron-impact dissociation of such adsorbates by both the primary beam electrons (with keV energy) and the emitted secondary electrons (with eV energy) results in metal-containing deposits and volatile reaction products, the latter being removed by the vacuum system. Advantageously, the same principle allows nanoscale removal of material. For example, physisorbed water on carbon surfaces dissociates under electron impact to produce highly reactive species that react to volatile carbon compounds, thus etching a nanosized hole in the substrate when a stationary focused electron beam is used.[9] Injected molecules used for electron-impact nanosynthesis so far comprise various metal–ligand compounds that contain carbon-, phosphorous-, or halogen-based ligands as well as organic compounds.[3] With the recent development of gas injection systems that allow the admission of two or more gases to the substrate surface, the nanosynthesis of binary metal alloys[10] or metal–(carbon) matrix deposits with outperforming properties[5c,e] can be envisaged. In contrast to classical vapor deposition exploiting co-evaporation, the deposit will be locally confined and the composition will depend not only on the ratios of molecule flow adsorption but also on the electron-impact dissociation efficiency of each individual molecule, giving a further degree of freedom to the control of tuned material synthesis.

Herein, we report on how to exploit electron exposure to tune the composition of a deposit when two adsorbates A and B contribute to electron-impact deposition. The principle is shown in Scheme 1 and starts from the reasonable assump-

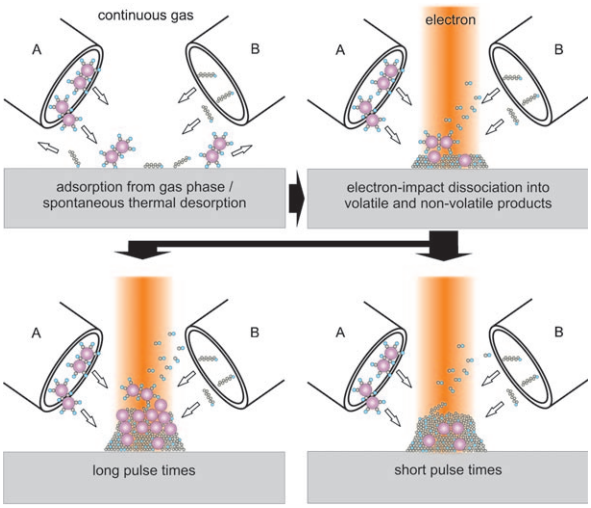

Scheme 1. Schematic representation of the two-adsorbate model. a) Before irradiation, competitive adsorption from the gas phase leads to an equilibrium surface density of both molecules according to their individual supply and desorption rates. b) Upon electron irradiation, the molecule with the larger electron-impact dissociation cross section is preferentially dissociated, say molecule B, and a B-rich deposit forms. Consequently, the adsorbate equilibrium shifts to become A-rich. c) If electron exposure continues, an A-rich deposit is obtained. d) If exposure is interrupted, the initial adsorbate equilibrium reestablishes, leading to a B-rich deposit upon the next exposure pulse.

[*] L. Bernau, Dr. M. Gabureac, Dr. I. Utke
Laboratory for Mechanics of Materials and Nanostructures
EMPA, Swiss Federal Laboratories for Materials Science and Technology, Feuerwerkerstrasse 39, 3602 Thun (Switzerland)
Fax: (+41) 332-284-490
E-mail: ivo.utke@empa.ch
Homepage: http://www.empa.ch/abt128
Dr. R. Erni
Electron Microscopy Center
EMPA, Swiss Federal Laboratories for Materials Science and Technology, Überlandstrasse 129, 8600 Dübendorf (Switzerland)

[**] This work was supported by the EC FP6 under Project BioNanoSwitch, grant no. 043288, and by COST Action CM0601.

Supporting information for this article is available on the WWW under http://dx.doi.org/10.1002/anie.201004220.

tions that both molecules reversibly co-adsorb (Scheme 1 a) and that electron-impact dissociation of each adsorbate species leads to deposition during an electron-beam exposure pulse (Scheme 1 b). Interestingly, the ratio of co-deposition can be controlled by varying the electron beam pulse duration in a specific time window defined by the adsorption and dissociation kinetics of the two adsorbates (Scheme 1 c,d). During the pulse interruption period, the focused electron beam can be moved to expose other (adjacent) positions on the substrate. By repeating the same exposure pattern, line or rectangle deposits with an internal nanocomposite structure may be fabricated at any desired thickness (Figure 1). The metal-to-carbon composition is seen to change considerably with the beam pulse period.

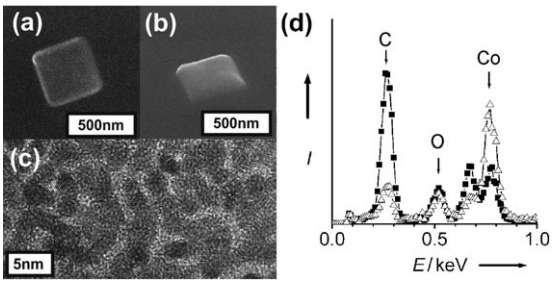

Figure 1. a) Scanning electron microscopy image of 600 nm square $[Co_2(CO)_8]$:hydrocarbon deposit in top view and b) tilted (45°) view. c) Transmission electron microscopy image of $[Co_2(CO)_8]$ deposit. The deposit material consists of Co nanocrystals (average diameter 2 nm) embedded in a carbonaceous matrix (light contrast). d) EDX spectra of two $[Co_2(CO)_8]$:hydrocarbon deposits (squares: 500 ns pulse time; triangles: 50 µs pulse time). The Co:C ratio varies from 0.3:1 (500 ns pulse time) to 3:1 (50 µs pulse time).

To model the change of composition with exposure parameters we considered the following generic electron-impact reactions of the two adsorbate species A and B giving nonvolatile reaction products D_A and D_B (the deposit) and volatile reaction products V_A and V_B [Eq. (1)].

$$A + e^- \rightarrow D_A + V_A + e^- \quad (1a)$$

$$B + e^- \rightarrow D_B + V_B + e^- \quad (1b)$$

The concentration of adsorbates A and B is described by their surface densities n_A and n_B (molecules per unit area). The evolution of n_A and n_B depends on the rates of molecule impingement (the local pressure), competitive adsorption, spontaneous thermal desorption, and electron-impact dissociation. It can be described by a system of inhomogeneous first-order differential equations [Eq. (2)]:

$$\frac{\partial n_A}{\partial t} = s_A J_A \left(1 - \frac{n_A}{n_{ML,A}} - \frac{n_B}{n_{ML,B}}\right) - \frac{n_A}{\tau_A} - \sigma_A f n_A \quad (2a)$$

$$\frac{\partial n_B}{\partial t} = s_B J_B \left(1 - \frac{n_A}{n_{ML,A}} - \frac{n_B}{n_{ML,B}}\right) - \frac{n_B}{\tau_B} - \sigma_B f n_B \quad (2b)$$

The first term in Equation (2) describes Langmuir surface adsorption accounting for surface adsorption sites already occupied by either species, the second term describes spontaneous thermal desorption, and the third term describes electron-impact dissociation. Here, s is the sticking probability, J is the flux of impinging molecules, τ is the adsorbate residence time, n_{ML} is the adsorbate surface density corresponding to complete monolayer coverage, and f is the primary electron flux; σ is the effective dissociation cross section and represents the convolution of the energy-dependent cross section with the energy distribution of all the electrons participating in the deposition process. Equations (2) can be solved analytically for n_A and n_B (see the Supporting Information, section B).

The number of adsorbate dissociations per primary electron, Y_A and Y_B, are given by Equation (3), where t_d is

$$Y_A = \sigma_A \int_0^{t_d} n_A(t)dt/t_d \quad (3a)$$

$$Y_B = \sigma_B \int_0^{t_d} n_B(t)dt/t_d \quad (3b)$$

the electron-beam pulse time (of irradiation) at a given position on the substrate surface. The deposit composition is given by Equation (4), where $[D_A]$ and $[D_B]$ are the concentrations of the nonvolatile dissociation products of the electron-impact reactions outlined in Equation (1). The range within which variation in composition can be realized by variation of the pulse time is given by Equation (5) (see the Supporting Information, section B).

$$Z = [D_A]/[D_B] = Y_A/Y_B \quad (4)$$

$$Z_{t_d \rightarrow 0} = \sigma_A s_A J_A \tau_A / \sigma_B s_B J_B \tau_B \quad (5a)$$

$$Z_{t_d \rightarrow \infty} = \sigma_A s_A J_A (1/\tau_B + \sigma_B f)/\sigma_B s_B J_B (1/\tau_A + \sigma_A f) \quad (5b)$$

$$Z_{t_d \rightarrow 0}/Z_{t_d \rightarrow \infty} = (1/f + \sigma_A \tau_A)/(1/f + \sigma_B \tau_B) \quad (5c)$$

From Equations (5), the following general statements can be derived: For very small exposure times [Eq. (5a)], both Equations (1a) and (1b) are electron-limited and the composition is proportional to the ratios of the electron-impact dissociation cross sections $\sigma_{A,B}$, the residence times $\tau_{A,B}$, the sticking probabilities $s_{A,B}$, and the molecule fluxes $J_{A,B}$ of both adsorbates. Furthermore, the composition is independent of the electron flux f for very small exposure times. For large exposure times [Eq. (5b)], it turns out that at least one of the electron-impact reactions must be driven into the molecule-limited regime to change the composition to a value different from that already obtained at very small exposure times [Eq. (5a)]. This requires adjustment of the electron flux such that $\sigma_A f \gg \tau_A^{-1}$ or $\sigma_B f \gg \tau_B^{-1}$. Equation (5c) highlights this condition and also illustrates that the larger the ratio $\sigma_A \tau_A / \sigma_B \tau_B$ the larger the range of tunable composition. A substrate temperature variation would exponentially change the residence times of both adsorbates according to their individual desorption energies. If these energies differ, Equations (5) predict a shift in composition upon substrate heating or cooling.

Below, we apply the above model to a two-adsorbate system typical of scanning electron microscopes where one functional molecule is injected into a high-vacuum chamber. Besides the functional molecule, there is hydrocarbon arising from the background chamber pressure of 10^{-5}–10^{-6} mbar. Rigid single-adsorbate conditions for electron-impact deposition can be realized in ultrahigh vacuum experiments.[11] Of note is that water is also present in high-vacuum, but it was found that water vapor must be present at very high pressures (>1 mbar) to have a net etching effect over hydrocarbon deposition and thus on the metal-to-carbon composition.[12] However, the presence of water could in some cases oxidize the deposited metal.[13] In our model, species A is a volatile metal compound [$Co_2(CO)_8$] and species B is a model hydrocarbon (octanol, $C_8H_{17}OH$).

To apply the above two-adsorbate model to the system [$Co_2(CO)_8$] and the model hydrocarbon, one needs to estimate the input parameters. The impinging molecular flux J was calculated from the background pressure for the hydrocarbon and from mass-loss measurements and Monte Carlo simulations for the injected [$Co_2(CO)_8$].[14] The monolayer density n_{ML} was estimated using the size of the molecule, and the sticking probability s was assumed unity. The residence time τ and the electron-impact dissociation cross section σ are a priori unknown molecular parameters. They were retrieved by fitting the deposition rates measured under quasi-single-adsorbate conditions (see the Supporting Information, section A). The values used are given in Table 1.

Table 1: Model parameters for [$Co_2(CO)_8$] and $C_8H_{17}OH$.

Molecule	sJ [$cm^{-2}s^{-1}$][a]	n_{ML} [nm^{-2}][b]	σ [nm^2][c]	τ [μs][c]
[$Co_2(CO)_8$]	1.5×10^{17}	2.6	4.95×10^{-3}	720
$C_8H_{17}OH$	1.6×10^{15}	3.4	2.1	190

[a] Calculated; [b] estimated from dimensions of intact molecule; [c] fit parameters from single-adsorbate experiments (see the Supporting Information, section A).

The integral of Equation (3) was solved numerically for varying electron-beam pulse times. The time between pulses allowed complete recovery of the initial adsorbate equilibrium from the gas phase. The corresponding dissociation yields for [$Co_2(CO)_8$] and the hydrocarbon are shown in Figure 2. The necessary conditions for a composition change derived from Equations (5a)–(5c) are fulfilled: as the electron-beam pulse time increases, the electron-impact reaction with hydrocarbon becomes molecule-limited at around 100 ns pulse time while the [$Co_2(CO)_8$] dissociation reaction remains electron-limited until about 40 μs. The corresponding Z values are calculated as $Z_{t_d\to0}=0.86$, $Z_{t_d\to\infty}=81$ and their ratio as 94, owing to the higher electron-impact dissociation cross section and the lower impingement rate of hydrocarbons (see Table 1).

The above Z values describe the concentration ratio of nonvolatile dissociation products D_A and D_B. Depending on the nature of the parent adsorbates, the dissociation products are either pure elements or compounds made up of additional elements from the parent adsorbate molecule.[15] Consequently, to allow comparison with measured compositions, the model needs to be adjusted to the compositions of D_A and D_B. Under our quasi-single-adsorbate conditions, the dissociation product of cobalt carbonyl adsorbates was approximately $Co_2C_{0.6}O_{0.4}$ for all exposure times. This composition represents the maximum obtainable metal content in our deposits (see the Supporting Information, section A). This result excludes the hypothesis of dissociation being more complete with respect to carbonyl ligands when the pulse time is increased in the present system. It is worth noting that pure cobalt deposits were obtained by using beam-induced heating or a heated substrate[16] and might be achieved under ultrahigh vacuum conditions (no water or hydrocarbon background) as was demonstrated for another carbonyl, [$Fe(CO)_5$].[11a,c] The discussion of these effects is beyond the scope of this article, but our model could account for either composition of D_A or D_B. The electron-impact dissociation product of the hydrocarbon adsorbates showed a carbon-to-oxygen ratio of about 8.5:1, which is similar to the ratio found in deposits from other organic precursors.[17] The compositional variation in the two-adsorbate system was then obtained from the average of the single adsorbate compositions weighted by the electron-impact dissociation yield (see section C of the Supporting Information for details). Figure 3 shows experimental composition values versus the electron beam pulse time; the two-adsorbate model derived above was found to be in excellent agreement.

In conclusion, the two-adsorbate model developed herein conceptually shows that tuning of deposit composition can be achieved by using pulsed electron beams. The tunable composition window is determined by the adsorption and supply rate of each adsorbate as well as their electron-impact

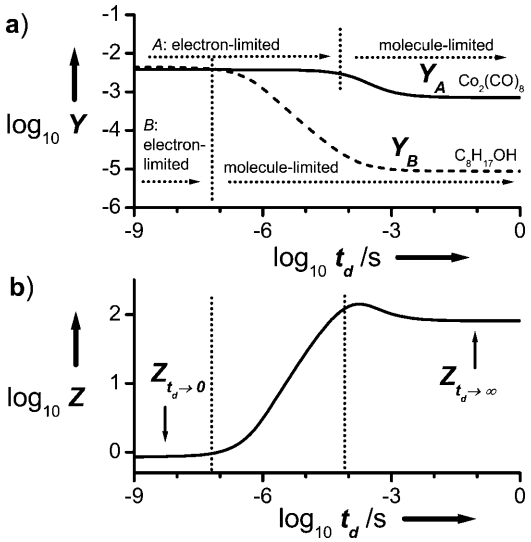

Figure 2. a) Calculated dissociation reaction yields Y (per primary electron) versus electron beam pulse time t_d for cobalt carbonyl (Y_A, solid line) and hydrocarbon (Y_B, dashed line), according to Equation (3) with the parameters given in Table 1. The individual regime transition from electron- to adsorbate-limited depends on the inequality $t_d > (sJ/n_{ML}+1/\tau+\sigma f)^{-1}$ (shown as dotted lines). b) Yield ratio Z (Eq. [4]); initial and final values depend on adsorption/desorption kinetics and electron-impact dissociation efficiency (Eq. [5]).

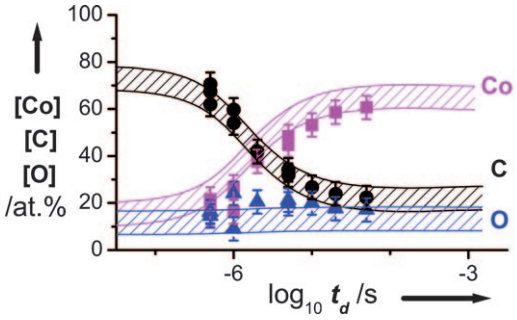

Figure 3. Measured composition of focused electron-beam-induced deposits versus electron-beam pulse time t_d (25 keV, 1 nA, 10 ms interruption period, $(600\ nm)^2$ square deposits) in the presence of two adsorbates $[Co_2(CO)_8]$ and hydrocarbon (squares: [Co]; circles: [C]; triangles: [O]). The prediction of the model is shown as an overlay taking $C_8H_{17}OH$ as model molecule for hydrocarbon.

efficiencies and their nonvolatile reaction products, which allows control of the compositions in nanosized deposits to tailor physical properties.[5c]

Specifically controlled cobalt–carbon compositions were obtained under high-vacuum conditions by varying the electron-exposure pulse times, and the model showed very good agreement with experimental data. The model could be refined by including surface diffusion as an adsorbate supply mechanism and by using Gaussian electron beam profiles in Equation (2).[18] This refinement will not change the general conclusions drawn above, as surface diffusion can be accounted for by an increased (effective) residence time. However, such a refined model would certainly permit the calculation of lateral composition gradients in the deposit.

Experimental Section

The focused electron-beam-induced experiments were carried out at room temperature in a Hitachi S-3600N scanning electron microscope, equipped with a tungsten filament electron source. Silicon substrates with a 200 nm thermal oxide layer were used as a substrate. Before deposition, the substrate was cleaned in acetone, rinsed with isopropanol, and blown dry with nitrogen. Homemade modifications to the microscope include an internal reservoir for the precursor, connected to a syringe nozzle pointed towards the substrate. Argon-stabilized dicobalt octacarbonyl ($[Co_2(CO)_8]$, CAS 10210–68–1, Merck Chemicals) was used as a precursor molecule.

The flow of $[Co_2(CO)_8]$ through the syringe nozzle (inner diameter 600 μm) was about 4.4×10^{15} moleculess^{-1}, as estimated from mass-loss measurements. According to our gas-flow MC simulations,[14] this flow translates into a flux of $1.5\times10^{17}\ cm^{-2}s^{-1}$ impinging $[Co_2(CO)_8]$ molecules within the irradiated substrate area. The dosage of the hydrocarbons was realized without a gas-injection system by simply pumping the vacuum chamber down to a residual chamber gas pressure of 1×10^{-5} mbar by using an oil diffusion pump system. This residual pressure is equal to $1.6\cdot10^{15}\ cm^{-2}s^{-1}$ homogeneously impinging model octanol hydrocarbons on the entire substrate surface.

Square deposits of $(600\ nm)^2$ were irradiated by a 25 keV, 1 nA electron beam with a full width at half maximum of 70 nm by moving the beam incrementally in a rectangular spiral pattern. The total irradiation dose was $10\ C\,cm^{-2}$. The beam was blanked for an interruption period of 10 ms between successive spiral scans to allow full replenishment of the surface with both adsorbate species.

The elemental composition of the deposits was characterized by energy-dispersive x-ray spectroscopy (EDX) at 3 keV. The accuracy of the compositional values obtained was checked to be correct to within ±5 at% by calibration measurements on cobalt carbonate ($CoCO_3$). Transmission electron microscopy (TEM) images were obtained on a JEOL 2200FS TEM/STEM instrument operated at 200 keV using an amorphous carbon membrane as deposition substrate.

Received: July 10, 2010
Published online: October 8, 2010

Keywords: adsorption · cobalt · electron microscopy · nanotechnology · surface chemistry

[1] K. E. Gonsalves, L. Merhari, H. Wu, Y. Hu, *Adv. Mater.* **2001**, *13*, 703–714.
[2] a) A. Turchanin, A. Beyer, C. T. Nottbohm, X. Zhang, R. Stosch, A. Sologubenko, J. Mayer, P. Hinze, T. Weimann, A. Gölzhäuser, *Adv. Mater.* **2009**, *21*, 1233–1237; b) T. R. Bedson, R. E. Palmer, J. P. Wilcoxon, *Microelectron. Eng.* **2001**, *57–58*, 837–841; c) E. U. Donev, J. T. Hastings, *Nano Lett.* **2009**, *9*, 2715–2718.
[3] a) I. Utke, A. Gölzhäuser, *Angew. Chem.* **2010**, DOI: 10.1002/ange.201002677; *Angew. Chem. Int. Ed.* **2010**, DOI: 10.1002/anie.201002677; b) I. Utke, P. Hoffmann, J. Melngailis, *J. Vac. Sci. Technol. B* **2008**, *26*, 1197; c) W. van Dorp, *J. Appl. Phys.* **2008**, *104*, 081301; d) S. J. Randolph, J. D. Fowlkes, P. D. Rack, *Crit. Rev. Solid State Mater. Sci.* **2006**, *31*, 55; e) A. Botman, J. J. L. Mulders, C. W. Hagen, *Nanotechnology* **2009**, *20*, 372001.
[4] a) S. Graells, S. Acimovic, G. Volpe, R. Quidant, *Plasmonics* **2010**, *5*, 135–139; b) H. W. P. Koops, O. E. Hoinkis, M. E. W. Honsberg, R. Schmidt, R. Blum, G. Böttger, A. Kuligk, C. Liguda, M. Eich, *Microelectron. Eng.* **2001**, *57–58*, 995–1001.
[5] a) K. Murakami, M. Takai, *J. Vac. Sci. Technol. B* **2004**, *22*, 1266–1268; b) T. Brintlinger, M. S. Fuhrer, J. Melngailis, I. Utke, T. Bret, A. Perentes, P. Hoffmann, M. Abourida, P. Doppelt, *J. Vac. Sci. Technol. B* **2005**, *23*, 3174–3177; c) M. Gabureac, L. Bernau, I. Utke, G. Boero, *Nanotechnology* **2010**, *21*, 115503; d) A. Fernández-Pacheco, J. M. de Teresa, R. Cordoba, M. R. Ibarra, D. Petit, D. E. Read, L. O'Brien, E. R. Lewis, H. T. Zeng, R. P. Cowburn, *Appl. Phys. Lett.* **2009**, *94*, 192509; e) M. Huth, D. Klingenberger, C. Grimm, F. Porrati, R. Sachser, *New J. Phys.* **2009**, *11*, 033032; f) G. C. Gazzadi, S. Frabboni, *J. Vac. Sci. Technol. B* **2005**, *23*, L1–L3.
[6] a) V. Friedli, I. Utke, K. Molhave, J. Michler, *Nanotechnology* **2009**, *20*, 385304; b) W. Ding, L. Calabri, X. Chen, K. M. Kohlhaas, R. S. Ruoff, *Compos. Sci. Technol.* **2006**, *66*, 1112–1124; c) S. Okada, T. Mukawa, R. Kobayashi, M. Ishida, Y. Ochiai, T. Kaito, S. Matsui, J.I Fujita, *Jpn. J. Appl. Phys.* **2006**, *45*, 5556–5559.
[7] a) R. Sharma, E. Moore, P. Rez, M. M. J. Treacy, *Nano Lett.* **2009**, *9*, 689–694; b) Y. M. Lau, P. C. Chee, J. T. L. Thong, V. Ng, *J. Vac. Sci. Technol. A* **2002**, *20*, 1295–1302.
[8] A. J. M. Mackus, J. J. L. Mulders, M. C. M. Van De Sanden, W. M. M. Kessels, *J. Appl. Phys.* **2010**, *107*, 116102.
[9] H. Miyazoe, I. Utke, J. Michler, K. Terashima, *Appl. Phys. Lett.* **2008**, *92*, 043124.
[10] R. C. Che, M. Takeguchi, M. Shimojo, W. Zhang, K. Furuya, *Appl. Phys. Lett.* **2005**, *87*, 223109.
[11] a) T. Lukasczyk, M. Schirmer, H. P. Steinruck, H. Marbach, *Small* **2008**, *4*, 841; b) J. D. Wnuk, J. M. Gorham, S. G. Rosenberg, W. F. van Dorp, T. E. Madey, C. W. Hagen, D. H. Fairbrother, *J. Appl. Phys.* **2010**, 107, 054301; c) M. W. Walz, M. Schirmer, F. Vollnhals, T. Lukasczyk, H. P. Steinruck, H. Marbach, *Angew. Chem.* **2010**, *122*, 4774–4778; *Angew. Chem. Int. Ed.* **2010**, *49*, 4669–4673.

[12] a) C. J. Lobo, M. Toth, R. Wagner, B. L. Thiel, M. Lysaght, *Nanotechnology* **2008**, *19*, 025303; b) M. Toth, C. J. Lobo, G. Hartigan, W. R. Knowles, *J. Appl. Phys.* **2007**, *101*, 054309.
[13] A. Perentes, G. Sinicco, G. Boero, B. Dwir, P. Hoffmann, *J. Vac. Sci. Technol. B* **2007**, *25*, 2228 – 2232.
[14] V. Friedli, I. Utke, *J. Phys. D* **2009**, *42*, 125305.
[15] a) L. G. Christophorou, J. K. Olthoff, *Fundamental Electron Interactions with Plasma Processing Gases*, Kluwer Academic, New York, **2004**; b) J. D. Wnuk, J. M. Gorham, S. G. Rosenberg, W. F. van Dorp, T. E. Madey, C. W. Hagen, D. H. Fairbrother, *J. Phys. Chem. C* **2009**, *113*, 2487 – 2496.
[16] a) A. Fernández-Pacheco, J. M. de Teresa, R. Cordoba, M. R. Ibarra, *J. Phys. D* **2009**, *42*, 055005; b) R. Córdoba, J. Sese, J. M. de Teresa, M. R. Ibarra, *Microelectron. Eng.* **2010**, *87*, 1550 – 1553.
[17] T. Bret, S. Mauron, I. Utke, P. Hoffmann, *Microelectron. Eng.* **2005**, *78–79*, 300 – 306.
[18] I. Utke, V. Friedli, M. Purrucker, J. Michler, *J. Vac. Sci. Technol. B* **2007**, *25*, 2219 – 2223.

